Next-to-leading order calculation of three-jet observables in hadron-hadron collisions

Zoltán Nagy*
Institute of Theoretical Science, 5203 University of Oregon, Eugene, Oregon 97403-5203, USA
(Received 24 July 2003; published 5 November 2003)

The production of three jets in hadron-hadron collisions is the first complex process which allows us to define a branch of variables in order to make more precise measurements of the strong coupling and the parton distribution function of the proton. This process is also suitable for studying the geometrical properties of the hadronic final state at hadron colliders. This requires a next-to-leading order prediction of the three-jet observables. In this paper we describe the theoretical formalism of such a calculation with sufficient detail. We use the dipole method to construct a Monte Carlo program for calculating three-jet observables at next-to-leading order accuracy. We present a theoretical prediction for inclusive and exclusive cross sections and for some relevant event shape variables such as the transverse thrust, transverse jet broadening, and E_{t3} variable.

DOI: 10.1103/PhysRevD.68.094002 PACS number(s): 13.87.Ce, 12.38.Bx

I. INTRODUCTION

In high-energy hadron-hadron collisions the processes with a purely hadronic final state is one of the clearest processes to test quantum chromodynamics (QCD) and measure its parameters simultaneously. According to perturbative QCD the cross section of this processes is a convolution of a long- and short-distance part.

The long-distance-dependent part is the parton distribution function of the incoming hadrons. This function is universal and process independent, and we can measure it in any basic process such as, for example, deep inelastic scattering.

The short-distance part is the partonic cross section that can be calculated in perturbative QCD as a function of a single parameter, the strong coupling (α_s). The main advantage of the hadronic final states at hadron-hadron colliders is that it is possible to measure the strong coupling and the parton distribution function (PDF) simultaneously.

The production of three jets is the first process which can provide a complex final state to define a branch of jet observables in order to be able to do more precise measurements of the strong coupling and give a better determination of the parton distribution function. On the other hand, this process allows us to do more advanced studies of the hadronic final states by measuring their geometrical properties. In order to be able to make quantitative predictions it is essential to perform the computations at least next-to-leading order (NLO) accuracy. In hadron collisions the most easily calculated one- and two-jet cross sections have so far been calculated at the NLO level [1,2]. At the next-to-leading level some inclusive three-jet observables were calculated by Giele and Kilgore [3,4] and by the author [5]. Furthermore, Trócsányi also calculated the three-jet cross section in an effective parton distribution function approximation [6].

The main difficulty of next-to-leading order calculations is the presence of singularities. In general, when evaluating higher-order QCD cross sections, one has to consider real-emission contributions and virtual corrections and one has to deal with different types of singularities. The ultraviolet singularities are present in the virtual contributions and they are removed by the renormalization. The infrared singularities are present in both the virtual and real contributions but the sum of them is finite. In the last few years theoretical developments have made possible next-to-leading order calculations for three-jet quantities. There are several general methods available for the cancellation of the infrared divergences that can be used for setting up a Monte Carlo program [7–9]. In computing the NLO correction we use the dipole formalism of Catani and Seymour [9], which we modified slightly in order to have better control of the numerical calculation. This scheme is discussed in detail in the next section.

The advantages of using the dipole method are the following: (i) no approximation is made; (ii) the exact phase space factorization allows full control over the efficient generation of the phase space; (iii) the use of neither color-ordered subamplitudes nor symmetrization nor partial fractioning of the matrix elements is required; (iv) Lorentz invariance is maintained, and therefore the switch between various frames can be achieved by simply transforming the momenta; (v) the use of crossing functions is avoided; (vi) it can be implemented in an actual program in a fully process-independent way.

The important theoretical development that made possible the three-jet calculation was that relevant one-loop amplitudes for the relevant subprocesses became available. For the $0\rightarrow gggg$ [10], $0\rightarrow q\bar{q}ggg$ subprocesses the amplitudes were calculated by Bern, Dixon, and Kosower [11] and for the $0\rightarrow q\bar{q}Q\bar{Q}g$ subprocess it was given by Kunszt, Signer, and Trócsányi [12]. Relevant six-parton tree-level matrix elements are also available [13–16].

In this paper we give sufficient details of our work and present several new results for next-to-leading order predictions of three-jet observables in hadron-hadron collisions that were not published before and they could be interesting in an experimental analysis. In Sec. II we give details of the analytic and numeric calculation and describe the structure of our result. In Sec. III we present complete NLO predictions for three-jet inclusive cross sections and their energy fraction distribution (Dalitz variables) using the inclusive $k_\perp$ algorithm [17] and the midcone algorithm [18]. We define the

*Email address: nagyz@physics.uoregon.edu; URL: http://www.cpt.dur.ac.uk/~nagyz/nlo++

thrust and jet broadening event shape variables in the transverse plane. We show some subjet result using the exclusive $k_\perp$ algorithm [19]. Section IV contains our conclusion.

II. DETAILS OF THE CALCULATION

A. Method

The next-to-leading order cross section for the process with two initial-state hadrons is the convolution of the parton density functions of the incoming hadrons and the hard scattering cross section,

$$\sigma(p,\overline{p}) = \sum_{a,b} \int_0^1 d\eta f_{a/H}(\eta,\mu_F^2) \int_0^1 d\overline{\eta} f_{b/\overline{H}}(\overline{\eta},\mu_F^2) \times [\sigma_{ab}^{LO}(\eta p, \overline{\eta p}) + \sigma_{ab}^{NLO}(\eta p, \overline{\eta p})], \quad (1)$$

where $f_{i/H}$ is the density of partons of type i in the incoming hadron H at the μ_F factorization scale. The corresponding parton-level cross sections are

$$\sigma_{ab}^{LO}(p,\overline{p}) \equiv \int_3 d\sigma_{ab}^B(p,\overline{p}) = \int_3 d\Gamma^{(3)} \langle |\mathcal{M}_{ab}^{(3)}|^2 \rangle F_J^{(3)}, \quad (2)$$

and the next-to-leading order correction is the sum of three integrals:

$$\sigma_{ab}^{NLO}(p,\overline{p}) \equiv \int d\sigma_{ab}^{NLO}(p,\overline{p}) = \int_4 d\sigma_{ab}^R(p,\overline{p}) + \int_3 d\sigma_{ab}^V(p,\overline{p}) + \int_3 d\sigma_{ab}^C(p,\overline{p}), \quad (3)$$

where $d\sigma^R$ and $d\sigma^V$ are the real and virtual contributions to the cross section. The contribution $d\sigma^C$ represents the collinear subtraction counterterm. The pole structure of this term is well defined but the finite part is factorization scale dependent. The actual form of the finite part in the expression of the $d\sigma^C$ defines the factorization scheme. In our calculations we chose the commonly used modified minimal subtraction ($\overline{\text{MS}}$) scheme. The parton density functions are also scheme dependent, so that this dependence cancels in the hadronic cross section of Eq. (1).

The three integrals on the right-hand side of Eq. (3) are separately divergent but their sum is finite provided by the jet function $F_J^{(m)}$, which defines an infrared-safe quantity, which formally means that

$$F_J^{(4)} \to F_J^{(3)}, \quad (4)$$

in any case where the four-parton and three-parton configurations are kinematically degenerate. The presence of singularities means that the separate pieces have to be regularized and the divergences have to be canceled. We use the dimensional regularization in $d=4-2\epsilon$ dimensions in which case the divergences are replaced double poles $1/\epsilon^2$ and single poles $1/\epsilon$. We assume that the ultraviolet renormalization of all Green functions to one-loop order has been carried out, so the divergences are infrared origin. In order to get the finite sum a slightly modified version of the Catani-Seymour [9] dipole method is used in our calculations.

The reason for modifying the original dipole formalism is numerical. The essence of the dipole method is to define a single subtraction term $d\sigma^A$, the dipole subtraction term, which regularizes the divergences in the real term which comes form the soft and collinear regions. Thus, the three singular integrals in Eq. (3) are substituted by three finite ones:

$$\sigma_{ab}^{NLO}(p,\overline{p}) = \sigma_{ab\{4\}}^{NLO}(p,\overline{p}) + \sigma_{ab\{3\}}^{NLO}(p,\overline{p}) + \int_0^1 dx [\hat{\sigma}_{ab\{3\}}^{NLO}(x,xp,\overline{p}) + \hat{\sigma}_{ab\{3\}}^{NLO}(x,p,x\overline{p})], \quad (5)$$

where the four-parton integral is given by

$$\sigma_{ab\{3\}}^{NLO}(p,\overline{p}) = \int_4 [d\sigma_{ab}^R(p,\overline{p})_{\epsilon=0} - d\sigma_{ab}^A(p,\overline{p})_{\epsilon=0}]. \quad (6)$$

We have two three-parton contributions to the NLO correction. The second term on the right-hand side of Eq. (5) is the sum of the one-loop contribution and a Born term convoluted by a universal singular factor **I**,

$$\sigma_{ab\{3\}}^{NLO}(p,\overline{p}) = \int_3 [d\sigma_{ab}^V(p,\overline{p}) + d\sigma_{ab}^B(p,\overline{p}) \otimes \mathbf{I}]_{\epsilon=0}. \quad (7)$$

The factor **I** contains all the ϵ poles which come from the $d\sigma^A$ and $d\sigma^C$ that are necessary to cancel the (equal and with opposite sign) poles in $d\sigma^V$. The last term in Eq. (5) is a finite remainder that is left after factorization of initial-state collinear singularities into the nonperturbative distribution functions (parton density function),

$$\int_0^1 dx \hat{\sigma}_{ab\{3\}}^{NLO}(x,xp,\overline{p}) = \sum_{a'} \int_0^1 dx \int_3 \{d\sigma_{a'b}^B(xp,\overline{p}) \otimes [\mathbf{P}(x) + \mathbf{K}(x)]^{aa'}\}_{\epsilon=0}, \quad (8)$$

where the x-dependent functions **P** and **K** are similar (but finite for $\epsilon \to 0$) to the factor **I**. These functions are universal; that is, they are independent of scattering process and of the jet observables.

There are several ways to define the $d\sigma^A$ dipole subtraction term, but all must lead to the same finite next-to-leading order correction. In this program a slight modification of the Catani-Seymour subtraction term was implemented by defining the dipole term as a function of a parameter $\alpha \in (0,1]$ which controls the volume of the dipole phase space. In the e^+e^- annihilation case this modification of the dipole formalism was discussed in Ref. [20], which we generalize for hadron-hadron collisions.

In this subsection we recall only those dipole factorization formulas that are relevant in our calculation. We do not want to give a precise definition of every variable, function, and factor; we just use the same notation of the original paper of the dipole method [9].

The $d\sigma^A$ local counterterm is provided by the dipole factorization of the tree-level squared matrix element. Thus we can define

$$d\sigma^A_{ab}=\sum_{\{4\}} d\Gamma^{(4)}(p_a,p_b,p_1,\ldots,p_4)\frac{1}{S_{\{4\}}}\Bigg\{\sum_{\substack{\text{pairs}\\ i,j}}\sum_{k\neq i,j}\mathcal{D}_{ij,k}(p_a,p_b,p_1,\ldots,p_4)F_J^{(3)}(p_a,p_b,p_1,\ldots,\tilde{p}_{ij},\tilde{p}_k,\ldots,p_4)$$

$$\times\Theta(y_{ij,k}<\alpha)+\sum_{\substack{\text{pairs}\\ i,j}}[\mathcal{D}^a_{ij}(p_a,p_b,p_1,\ldots,p_4)F_J^{(3)}(\tilde{p}_a,p_b,p_1,\ldots,\tilde{p}_{ij},\ldots,p_4)\Theta(1-x_{ij,a}<\alpha)+(a\leftrightarrow b)]$$

$$+\sum_{i\neq k}[\mathcal{D}^{ai}_k(p_a,p_b,p_1,\ldots,p_4)F_J^{(3)}(\tilde{p}_a,p_b,p_1,\ldots,\tilde{p}_k,\ldots,p_4)\Theta(u_i<\alpha)+(a\leftrightarrow b)]$$

$$+\sum_i[\mathcal{D}^{ai,b}(p_a,p_b,p_1,\ldots,p_4)F_J^{(3)}(\tilde{p}_a,p_b,\tilde{p}_1,\ldots,\tilde{p}_4)\Theta(\tilde{v}_i<\alpha)+(a\leftrightarrow b)]\Bigg\}, \tag{9}$$

where $d\Gamma^{(4)}$ is the four-parton phase space including all the factors that are QCD independent, $\Sigma_{\{4\}}$ denotes the sum over all the configurations with four partons, and $S_{\{4\}}$ is the Bose symmetry factor of identical partons in the final state. The $\mathcal{D}_{ij,k}$, $\mathcal{D}^a_{ij}$, $\mathcal{D}^{ai}_k$, and $\mathcal{D}^{ai,b}$ are the dipole terms. The function $F_J^{(3)}$ is the jet function which acts over the three-parton dipole phase space. The $y_{ij,k}$, $x_{ij,a}$, u_i, $\tilde{v}_i$ are dipole variables defined by dipole factorization of the phase space. The dipole factorization of the phase space is exact phase space factorization which means that there is no approximation used in the kinematically degenerated regions (soft, collinear, and soft-collinear). We found that it makes the Monte Carlo integral more stable because the real contribution and subtraction terms are defined in same phase space point.

In Eq. (9) the $\alpha=1$ case means full dipole subtraction and it gives back the original dipole subtraction terms. In a computer program the large number of dipoles terms and complicated analytic structure of the expressions makes evaluation of the subtraction terms rather time consuming. Using this cut dipole phase space we can speed up the program. The parameter α is also useful to check our program by varying the value of α and checking whether the full correction is independent of this parameter.

The most serious numerical defect of the subtraction schemes is the missed binning. This happens when a huge positive weight from the real part and the corresponding huge negative weight that form the subtraction term are filled into different histogram bins. It is obvious that this cut can increase the numerical stability of the Monte Carlo program by decreasing the size of the dipole phase space which reduces the chance of the missed binning.

The introduced α phase space cut parameter requires one to redefine the $\mathbf{I}$ and $\mathbf{K}(x)$ flavor kernels. The singular factor $\mathbf{I}$ is given by

$$\mathbf{I}(p_1,\ldots,p_m;\alpha;\epsilon)$$

$$=-\frac{\alpha_s}{2\pi}\frac{1}{\Gamma(1-\epsilon)}\sum_I\frac{1}{\mathbf{T}_I^2}\mathcal{V}_I(\alpha,\epsilon)\sum_{J\neq I}\mathbf{T}_I\cdot\mathbf{T}_J\left(\frac{4\pi\mu^2}{2p_Ip_J}\right)^{\epsilon}, \tag{10}$$

where the indices I,J run over both final- and initial-state partons and the $p_I\cdot p_J$ dot products are always positive and

$$\mathcal{V}_i(\alpha,\epsilon)=\mathbf{T}_i^2\left(\frac{1}{\epsilon^2}-\frac{\pi^2}{3}\right)+\gamma_i\frac{1}{\epsilon}+\gamma_i+K_i(\alpha)+\mathcal{O}(\epsilon), \tag{11}$$

where

$$K_i(\alpha)=K_i-\mathbf{T}_i^2\ln^2\alpha+\gamma_i(\alpha-1-\ln\alpha). \tag{12}$$

The K_i and γ_i constants are defined in Eqs. (5.90) and (7.28) in Ref. [9]. The $\mathbf{K}(x,\alpha)$ flavor kernel is given by

$$\mathbf{K}^{a,a'}(x,\alpha)$$

$$=\frac{\alpha_s}{2\pi}\Bigg\{\overline{K}^{aa'}(x,\alpha)-K_{FS}^{aa'}(x)-\mathbf{T}_b\cdot\mathbf{T}_{a'}\frac{1}{\mathbf{T}_{a'}^2}\tilde{K}^{aa'}(x,\alpha)$$

$$+\delta^{aa'}\sum_i\mathbf{T}_i\cdot\mathbf{T}_a\frac{\gamma_i}{\mathbf{T}_i^2}\left[\left(\frac{1}{1-x}\right)_{1-\alpha}+\alpha\delta(1-x)\right]\Bigg\}, \tag{13}$$

where $K_{FS}^{aa'}(x)$ is defined by the factorization scheme. In the case of the $\overline{\text{MS}}$ scheme these functions are identically zero. The flavor functions $\overline{K}^{ab}(x,\alpha)$ are

$$\overline{K}^{ab}(x,\alpha)$$

$$=\hat{P}'_{ab}(x)+P^{ab}_{reg}(x)\ln\frac{\alpha(1-x)}{x}+\delta^{ab}\mathbf{T}_a^2\delta(1-x)\ln^2\alpha$$

$$+\delta^{ab}\Bigg[\mathbf{T}_a^2\left(\frac{2}{1-x}\ln\frac{1-x}{x}\right)_+$$

$$-\delta(1-x)\left(\gamma_a+K_a(\alpha)-\frac{5}{6}\pi^2\mathbf{T}_a^2\right)\Bigg]$$

$$+\delta^{ab}\mathbf{T}_a^2\frac{2}{1-x}\left(\ln\frac{\alpha(2-x)}{1+\alpha-x}-\ln\frac{2-x}{1-x}\Theta(x<1-\alpha)\right). \tag{14}$$

The $\tilde{K}^{ab}(x,\alpha)$ flavor kernels are defined by

$$\tilde{K}^{ab}(x,\alpha)=P^{ab}_{reg}(x)\ln\frac{1-x}{\alpha}+\langle\hat{P}_{a,b}(x,\epsilon=0)\rangle\ln\alpha(x)$$
$$-\delta^{ab}\mathbf{T}_a^2\left[\left(\frac{2}{1-x}\ln\frac{1}{1-x}\right)_{1-\alpha}+\frac{\pi^2}{3}\delta(1-x)\right]$$
$$+\delta^{ab}\mathbf{T}_a^2\frac{2}{1-x}\left[\ln\frac{1+\alpha-x}{\alpha}\right.$$
$$\left.-\ln(2-x)\Theta(x>1-\alpha)\right], \quad (15)$$

where the function $\alpha(x)$ is given by

$$\alpha(x)=\min\left\{1,\frac{\alpha}{1-x}\right\}. \quad (16)$$

The definitions of the Altarelli-Parisi probabilities $[P^{ab}_{reg}(x),\ \hat{P}'_{ab}(x)]$ and splitting functions ($\langle\hat{P}_{a,b}(x,\epsilon)\rangle$) are given in Appendix C in Ref. [9]. The "$\beta=1-\alpha$" prescription is defined by

$$\int_0^1 dx\left(\frac{1}{1-x}\right)_\beta f(x)=\int_\beta^1 dx\frac{f(x)-f(1)}{1-x}. \quad (17)$$

B. Structure of the results

Once the phase space integrations are carried out, we write the NLO jet cross section in the form

$$\sigma^{n\text{jet}}_{AB}=\sum_{a,b}\int_0^1 d\eta\int_0^1 d\bar{\eta}f_{a/A}(\eta,\mu_F^2)f_{b/B}(\bar{\eta},\mu_F^2)$$
$$\times\hat{\sigma}^{n\text{jet}}_{ab}[p_a,p_b,\alpha_s(\mu_R^2),\mu_R^2/Q^2_{HS},\mu_F^2/Q^2_{HS}], \quad (18)$$

where $f_{i/H}(\eta,\mu_F^2)$ represents the patron distribution function of the incoming hadron defined at the factorization scale $\mu_F=x_FQ_{HS}$, $\eta_{a,b}$ is the fraction of the proton momentum carried by the scattered partons $p_{a,b}$, Q_{HS} is the hard scale that characterizes the parton scattering which could be E_T of the jet, jet mass of the event, etc., and $\mu_R=x_RQ_{HS}$ is the renormalization scale.

In the presented leading and next-to-leading order results we use the C/C++ implementation [21] of the LHAPDF library [22] with CTEQ6 [23] parton distribution function and with the corresponding α_s expression which is included in this library. The CTEQ6 set was fitted using the two-loop running coupling with $\alpha_s(M_{Z^0})=0.118$.

To ensure the correctness of the result several checks were performed: (i) the Born-level two-, three-, and for-jet cross sections were compared to the prediction of the NJETS [16] program and perfect agreement was found; (ii) the singular behavior of the real and dipole subtraction terms was checked numerically in randomly chosen phase space points; (iii) the total NLO correction was independent of the α parameters that control the dipole phase space; (iv) the program is based on the NLOJET++ program library [21], which was used in other already well-tested processes.

In the NLO calculation the difference of the real contributions and the dipole subtraction terms is still singular but these are integrable square-root singularities. Integrating these singularities by a simple Monte Carlo integration technique (choosing random values of the integration variables uniformly) is not an efficient way because the variance of the estimate of the integral is infinite and we are not able to estimate the statistical error of the integral. To improve the stability and convergence of the Monte Carlo integral the phase space is generated by a multichannel weighted phase space generator [24].

III. RESULTS

In this section we study those jet observables which could be interesting in jet studies at hadron-hadron colliders. We show some examples of inclusive three-jet cross sections, energy fraction distributions of the jets, event shapes variables, and subjet rates. To present inclusive jet cross sections and some related jet observables like the energy fraction distribution we use the Ellis-Soper inclusive $k_\perp$ algorithm [17] and the midpoint cone algorithm [18]. To do subjet studies and calculate some jet-clustering algorithm-related event shape variables like the flipping variable we use the exclusive $k_\perp$ algorithm which was defined by Catani *et al.* in Ref. [19]. We also present some jet-clustering-independent event shape distributions which are defined in the transverse plane (transverse thrust and transverse jet broadening).

A. Three-jet inclusive cross sections

The most important jet quantities are the inclusive jet cross section and its transverse distribution. In hadron-hadron collisions for jet studies a variant of the cone algorithms was used. Unfortunately those algorithms which were used at the first run of the Tevatron are infrared and/or collinear unsafe or only safe up to a given order in the perturbative calculation. It is essential that the used jet algorithm to be infrared safe at all orders; otherwise, the perturbative calculation and the perturbative prediction are unstable. Using an *almost*-infrared-unsafe jet algorithm we are not able to estimate the effect of the higher-order contributions due to the variation of the renormalization and factorization scales. The other problem with this type of jet algorithms is that they are logarithmically sensitive to the detector resolution (energy and angular resolution). That is bad because in the fixed-order perturbative calculation it is impossible or difficult to consider or simulate precisely these effects [25].

In this subsection we use the Ellis-Soper inclusive $k_\perp$ algorithm and the midcone iterative cone algorithm which are infrared and collinear safe to all orders. In both cases we consider only those jets as hard final-state jets which have at least 20 GeV transverse energy and are in the $|\eta|<2$ pseudorapidity interval. The total jet transverse energy must be larger than 80 GeV. The renormalization and factorization scales are characterized by the hard scale which is a third of the total jet transverse momentum:

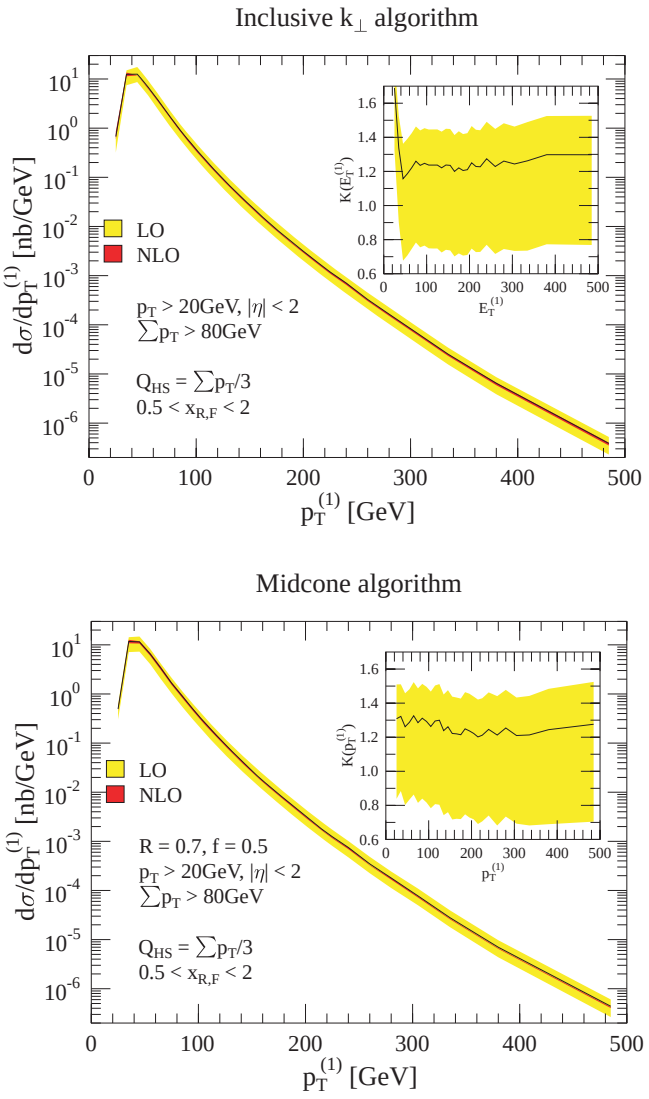

FIG. 1. (Color online) The fixed-order QCD predictions for the inclusive three-jet differential cross sections of the transverse momentum of the leading jet obtained using the inclusive $k_\perp$ and midcone algorithms. The bands indicate the theoretical uncertainty due to the variation of the scales $x_{R,F}$ between 0.5 and 2. The gray band is the leading order and the dark gray band is the next-to-leading order. The insets show the K factor and its scale dependence. The solid line represents the $x_{R,F}=1$ scale choice.

$$Q_{HS}=\frac{1}{3}\sum_{j=1}^{n_J} p_T^{\text{jet}}(j). \tag{19}$$

All jets contribute to this sum which passed the cuts.

Calculating the transverse energy distribution of the leading jet and comparing the leading and next-to-leading order fixed-order predictions we can see in the $k_\perp$ case, if the scales are set to $x_{R,F}=1$, the NLO correction is about 25%–30% as shown in Fig. 1. The $K=\sigma^{NLO}/\sigma^{LO}$ factor strongly depends on the scale choice but the NLO prediction is stable. Varying the scales between 0.5 and 2 the scale uncertainty of the NLO prediction is about 8%–10% which is significantly smaller than the leading order uncertainty which is about 100% or more.

TABLE I. Next-to-leading order results for the differential distribution of the three-jet inclusive cross sections as a function of the transverse energy of the leading jet. The scales are $x_{R,F}=1$. The errors are the statistical error of the Monte Carlo integration.

$E_T^{(1)}$ (GeV)	$k_\perp$ algorithm (nb/GeV)	Midcone algorithm (nb/GeV)
20–30	$(6.745\pm0.240)\times10^{-1}$	$(4.961\pm0.387)\times10^{-1}$
30–40	$(1.245\pm0.009)\times10^{1}$	$(1.174\pm0.019)\times10^{1}$
40–50	$(1.252\pm0.009)\times10^{1}$	$(1.148\pm0.014)\times10^{1}$
50–60	$(6.966\pm0.042)\times10^{0}$	$(6.522\pm0.077)\times10^{0}$
60–70	$(3.509\pm0.020)\times10^{0}$	$(3.338\pm0.034)\times10^{0}$
70–80	$(1.799\pm0.009)\times10^{0}$	$(1.662\pm0.017)\times10^{0}$
80–90	$(9.175\pm0.049)\times10^{-1}$	$(9.003\pm0.096)\times10^{-1}$
90–100	$(4.991\pm0.026)\times10^{-1}$	$(4.884\pm0.054)\times10^{-1}$
100–110	$(2.755\pm0.015)\times10^{-1}$	$(2.713\pm0.028)\times10^{-1}$
110–120	$(1.583\pm0.009)\times10^{-1}$	$(1.595\pm0.018)\times10^{-1}$
120–130	$(9.362\pm0.057)\times10^{-2}$	$(9.452\pm0.011)\times10^{-2}$
130–140	$(5.554\pm0.035)\times10^{-2}$	$(5.607\pm0.069)\times10^{-2}$
140–150	$(3.461\pm0.022)\times10^{-2}$	$(3.517\pm0.045)\times10^{-2}$
150–160	$(2.164\pm0.015)\times10^{-2}$	$(2.152\pm0.030)\times10^{-2}$
160–170	$(1.350\pm0.010)\times10^{-2}$	$(1.398\pm0.019)\times10^{-2}$
170–180	$(8.784\pm0.068)\times10^{-3}$	$(9.103\pm0.135)\times10^{-3}$
180–190	$(5.725\pm0.049)\times10^{-3}$	$(6.110\pm0.099)\times10^{-3}$
190–200	$(3.806\pm0.032)\times10^{-3}$	$(4.014\pm0.065)\times10^{-3}$
200–210	$(2.592\pm0.022)\times10^{-3}$	$(2.698\pm0.048)\times10^{-3}$
210–220	$(1.740\pm0.016)\times10^{-3}$	$(1.786\pm0.034)\times10^{-3}$
220–230	$(1.185\pm0.011)\times10^{-3}$	$(1.243\pm0.025)\times10^{-3}$
230–250	$(7.048\pm0.057)\times10^{-4}$	$(7.503\pm0.121)\times10^{-4}$
250–270	$(3.270\pm0.036)\times10^{-4}$	$(3.471\pm0.080)\times10^{-4}$
270–290	$(1.646\pm0.020)\times10^{-4}$	$(1.797\pm0.042)\times10^{-4}$
290–320	$(7.041\pm0.068)\times10^{-5}$	$(7.754\pm0.155)\times10^{-5}$
320–350	$(2.530\pm0.031)\times10^{-5}$	$(2.781\pm0.057)\times10^{-5}$
350–410	$(6.471\pm0.064)\times10^{-6}$	$(6.993\pm0.129)\times10^{-6}$
410–560	$(3.864\pm0.044)\times10^{-7}$	$(4.391\pm0.096)\times10^{-7}$

Using the midcone algorithm we got a very similar result. In this calculation the cone size is $R=0.7$ and the merge and split threshold parameter is $f=0.5$. In this case the NLO correction is about 20%–30% with the $x_{R,F}=1$ scales.

In Table I the NLO cross sections are tabulated. Comparing the values we can see that the $k_\perp$ algorithm gives a higher cross section in the low-E_T region while in the high-E_T region the cone result is higher. The difference between the two results is less than 10% almost everywhere.

B. Topology of the three-jet events

One can study the structure of the three-jet events. We can define variables which test certain properties of the jets. These quantities could be any azimuthal correlation between the jets or the energy fraction of the three leading jets.

The energy fraction of the three leading jets (leading in transverse energy) was measured by the CDF Collaboration [26,27]. This quantity is defined in the center-of-mass frame

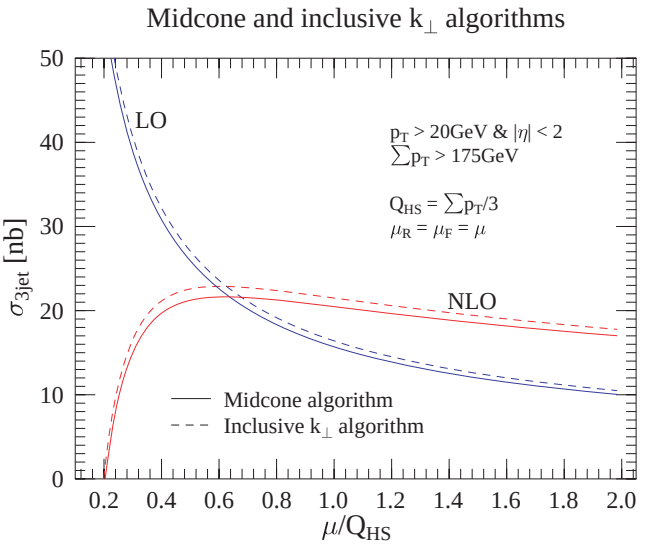

FIG. 2. (Color online) The scale dependence of the total three-jet cross sections.

of the three jets. The jets are ordered and labeled by energy in the rest frame ($E_1 > E_2 > E_3$). The energy fraction variables (usually called Dalitz variables) are given by

$$X_i = \frac{2E_i}{E_1 + E_2 + E_3}, \quad i = 1,2,3. \tag{20}$$

The variable X_1 varies between 2/3 and 1, X_2 between 1/2 and 1, and X_3 between 0 and 2/3. There are only two independent variables since $X_1 + X_2 + X_3 = 2$. We use only the first two variables.

In the experimental analysis the iterative cone algorithm was used with an additional cut on the jets. It was required that the jets be well separated. This additional cut ensures that the cross section is calculable order by order in perturbation theory but the jet algorithm is still not fully infrared safe; it is almost infrared unsafe [25].

To get stable theoretical predictions in our calculations we use the inclusive $k_\perp$ and midcone jet algorithms to resolve jets with the same cuts that were used in Ref. [27]. All jets are required to have at least 20 GeV transverse energy and they must lie in the $|\eta| < 2$ pseudorapidity window. We calculate the normalized differential distributions of the X_1 and X_2 variables and the double differential distribution of these variables. In these calculations the renormalization and factorization scales are set to a third of the total jet transverse energy, Eq. (19).

The distributions are normalized by the total three-jet cross section plotted in Fig. 2. We can see that the NLO correction reduced the scale dependence of the perturbative prediction. The scale uncertainty of the NLO result is about 10%–12%, varying the scales in the $0.6 < x_{R,F} < 2$ range, while the LO uncertainty is much higher, 38%–40%. The corrections with the $x_{R,F} = 1$ scale choice are about 30%.

The double differential distributions of the variables X_1 and X_2 are plotted in Fig. 3. The phase space would populate

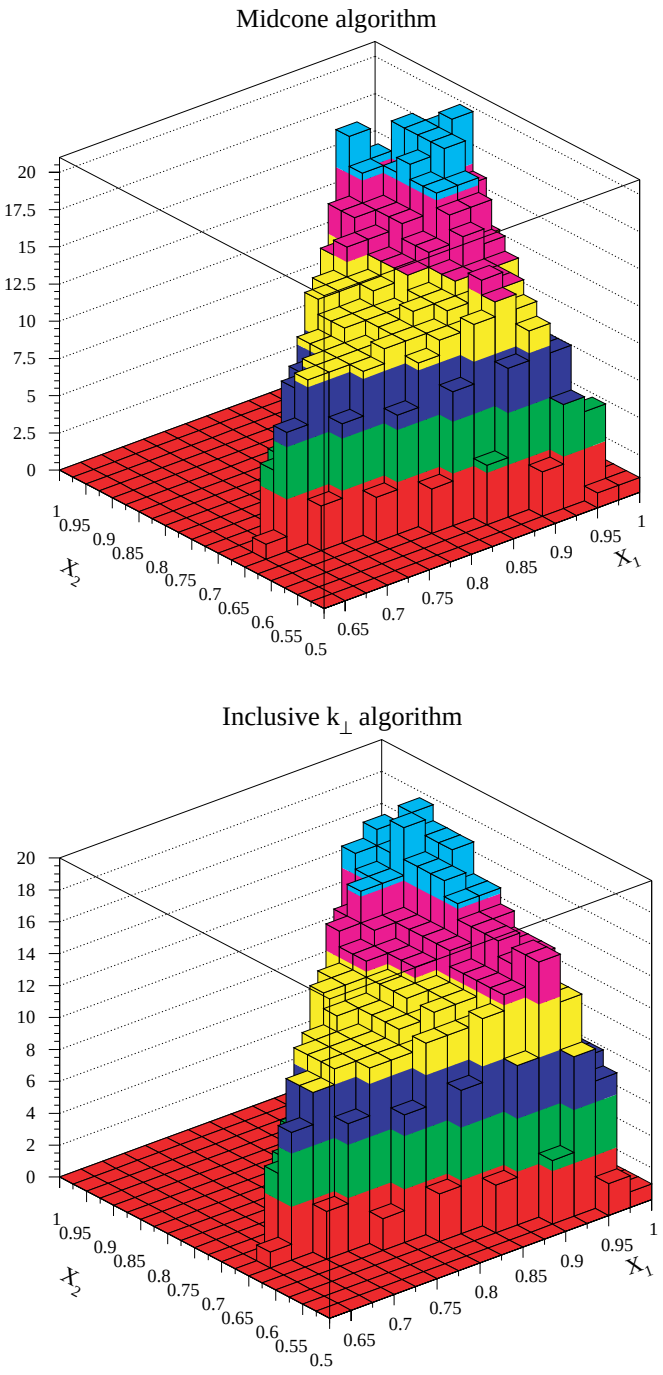

FIG. 3. (Color online) Next-to-leading order perturbative prediction for the normalized double differential distribution $(1/\sigma d\sigma/dX_1 dX_2)$ of the energy fraction variables X_1 and X_2 using the midcone and inclusive $k_\perp$ algorithms.

the available X_1, X_2 region uniformly. Deviation from the uniform distribution shows the effect of the QCD dynamics.

Taking the double differential distribution and projecting on either axis the distributions of variables X_1 and X_2 can be obtained. In Fig. 4 the differential distributions of the energy fractions are plotted in the inclusive $k_\perp$ and midcone algorithm cases.

Comparing the leading order result to the next-to-leading order result we can see that the NLO distribution of the lead-

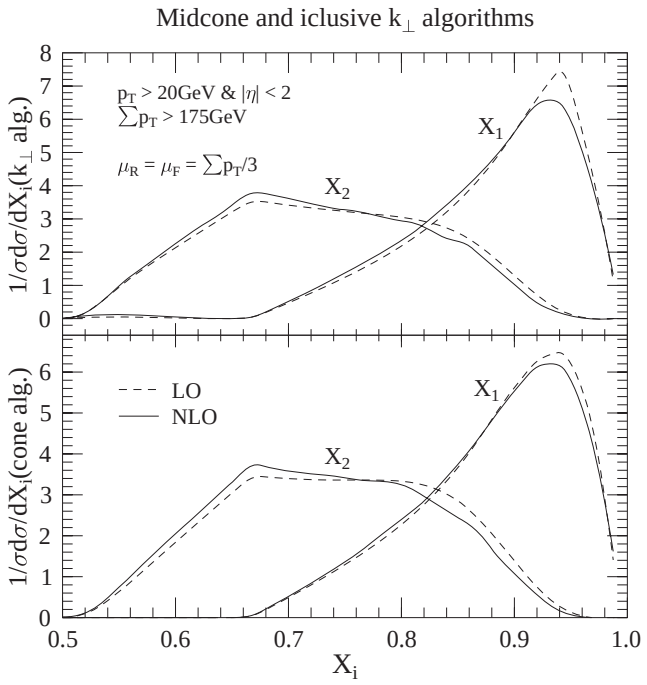

FIG. 4. The energy fraction distribution of the leading (X_1) and second leading (X_2) jets. The upper figure is result with the inclusive $k_\perp$ algorithm and the lower figures shows the midcone result.

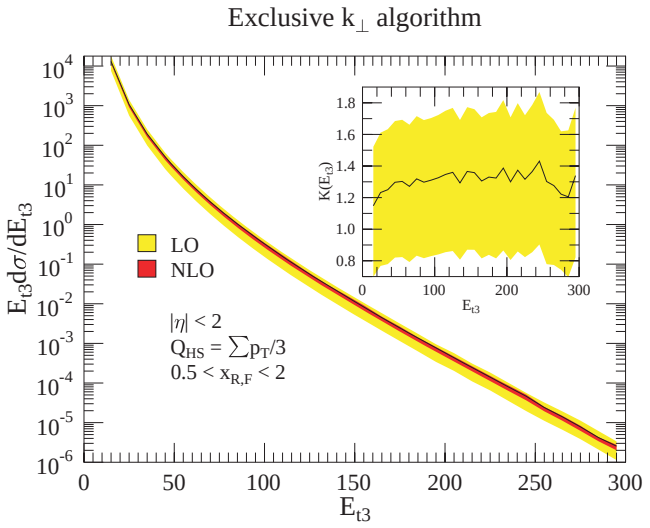

FIG. 5. (Color online) Distribution of the E_{t3} event shape variable at the LO an NLO levels. The bands indicate the theoretical uncertainty due to the variation of the scales $x_{R,F}$ between 0.5 and 2. The gray band is the leading order and the black band is the next-to-leading order. The inset shows the K factor and its scale dependence. The solid line represents the $x_{R,F}=1$ scale choice.

ing jet is less peaked than the LO but in the case of the X_2 distribution the NLO result is more peaked around 0.65. The NLO correction of the distributions is small.

Comparing the two algorithms to each other we can say that the distributions are very similar and there is not too much difference. The X_1 distribution of the inclusive $k_\perp$ algorithm is a little bit more peaked and the X_2 distribution is a little bit flatter than in the midcone case. The corresponding peaks are in the same positions.

C. Three-jet event shapes

We can distinguish two types of event shapes. One can calculate and measure the event shapes which are associated with a jet algorithm. Generally we can say that this type of variable gives information about any geometrical property of the jets in an n-jet event. Or we can define event shape variables which measure any geometrical property of the event: e.g., thrust or jet bordering.

Using the exclusive $k_\perp$ algorithm there is a natural way to introduce event shape variables. The prescription of this algorithm introduces a stopping parameter d_{cut} (resolution variable), which defines the hard scale of the process and separates the event into a hard scattering part and a low-p_T part (*beam jet*).

Defining the d_{cut} resolution variable event by event we can calculate the differential distribution of the E_{tn} event shape variable. Denoting by d_m the smallest resolution variable when the event has m hard final state jets the E_{tn} event shape variable is defined by

$$E_{tn}^2 = \max_{m \geqslant n}\{d_m\}. \tag{21}$$

We plot the differential distribution of the E_{t3} event shape variable in Fig. 5. In this calculation the $|\eta|<2$ pseudorapidity cut was applied for every hard final state jet. The renormalization and factorization scales were given by $\mu_{R,F}=x_{R,F}Q_{HS}$ where the hard scale is the average transverse momentum of the three jets:

$$Q_{HS}=\frac{1}{3}\sum_{j=1}^{3} p_T^{\text{jet}}(j). \tag{22}$$

Comparing the next-to-leading order result to the leading order result we see that the LO prediction strongly depends on the scales. Varying the scale parameters $x_{R,F}$ between 0.5 and 2 the scale uncertainty of the NLO result is about 15% in contrast to the LO scale uncertainty which is about 80%. Setting the scales to $x_{R,F}=1$ we see that the NLO correction is about 20%–35%.

One can define event shapes on the transverse plane. An important example is the transverse thrust which is defined by

$$T_\perp = \max_{\vec{n}} \frac{\sum_{i \in C_N} |\vec{p}_{\perp,i}\cdot\vec{n}|}{\sum_{i \in C_N} |\vec{p}_{\perp,i}|}, \tag{23}$$

where $\vec{p}_{\perp,i}$ is the transverse component of the parton (hadron) momentum. The unit vector that $\vec{n}$ maximizes the ratios of the sums is usually called the thrust axis. In these sums only those particles are counted which fulfill all selection

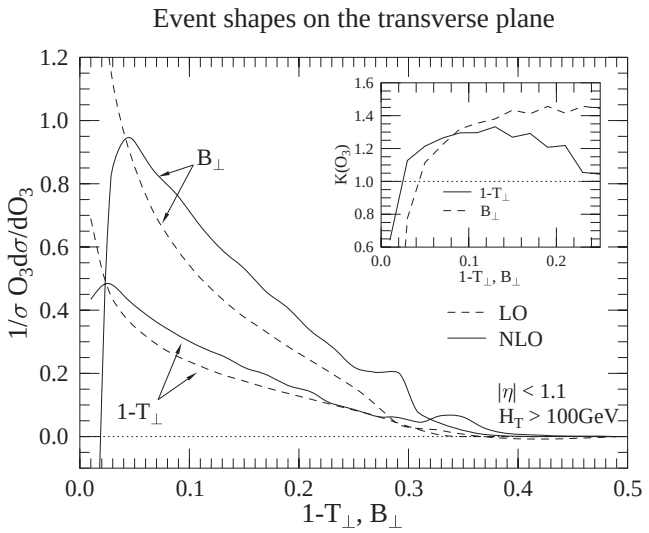

FIG. 6. Distribution of $1-T_\perp$ and $B_\perp$ event shape variables at the LO (*dashed line*) and NLO (*solid line*) levels. The scales were set to $\mu_{R,F}=H_T$. The inset shows the K factors.

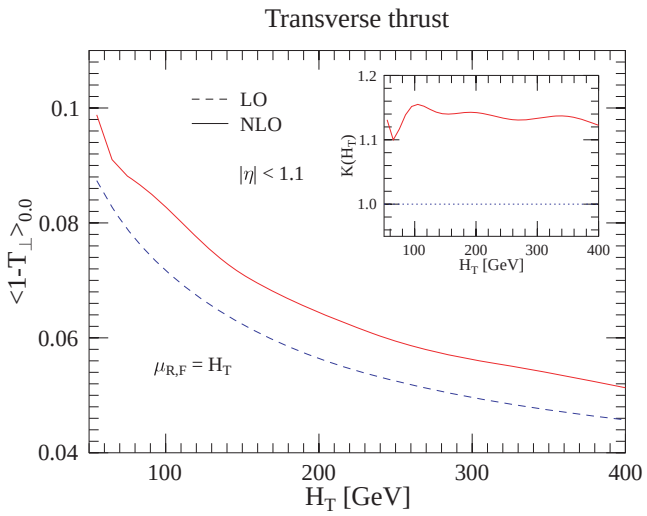

FIG. 7. (Color online) Average value of the $1-T_\perp$ event shape variable at $\delta=0$ at the LO (*dashed line*) and NLO (*solid line*) levels. The scales were set to $\mu_{R,F}=H_T$. The inset shows the K factor.

criteria C_N. This selection must be infrared safe. In this calculation we required that the pseudorapidity of those particles which contribute to $T_\perp$ be in the $[-1.1,1.1]$ pseudorapidity window; thus, we have

$$C_N=\{i:\ |\eta_i|<1.1,\ i=1,\ldots,N\}, \tag{24}$$

where N is the number of particles in the event. This definition of the thrust for hadron colliders gives an infrared-safe longitudinally boost-invariant quantity.

The jet broadening $B_\perp$ is an associated quantity to the thrust. Using the thrust axis we can define $B_\perp$ on the transverse plane by the formulas

$$B_\perp=\frac{\sum_{i\in C_N}|\vec{p}_{\perp,i}\times\vec{n}|}{2\sum_{i\in C_N}|\vec{p}_{\perp,i}|}. \tag{25}$$

In Fig. 6 the differential distributions of the transverse thrust and transverse jet broadening are plotted at the LO and NLO levels. In this calculation the total transverse energy is larger than 100 GeV:

$$H_T\equiv\sum_{i\in C_N}E_{T,i}>100\ \text{GeV}. \tag{26}$$

The perturbative results are logarithmically divergent at the edge of the phase space. This divergence occurs at $T_\perp=1$ and $T=2/3$ in the thrust distribution and at $B_\perp=0$ and $B=1/3$ in the jet broadening distribution. Setting the scale to the total transverse energy the NLO order correction in the middle of the distribution where the effect of the logarithm is small is 30%–35% for the thrust and 20%–45% for jet broadening as is shown in the inset. It is necessary to do an all-order resummation of the leading and next-to-leading logarithms to be able to do a quantitative comparison of the theory to the data.

One can define the average value of the event shape variables as a function of the total transverse energy. This quantity is given by the ratio

$$\langle O_3\rangle_\delta=\left(\frac{d\sigma}{dH_T}\right)^{-1}\int_\delta^1 dO_3 O_3\frac{d\sigma}{dO_3 dH_T}, \tag{27}$$

where O_3 could be either $1-T_\perp$ or $B_\perp$.

Figure 7 shows the average value of the transverse thrust. With the $\mu_{R,F}=H_T$ scale choice it was found that the NLO correction is small, about 15%. The NLO correction does not change the shape of the distribution as is shown by the K-factor plot. This result indicates that the NLO fixed-order prediction might describe the data with good accuracy.

Figure 8 shows the average value of the transverse jet broadening. The CDF collaboration [28] measured this distribution with the $\delta=0$ choice and the data were compared to the leading order QCD prediction. Comparing the data to the NLO prediction the difference between the data and theory is huge. This can happen because the contribution of large logarithms from the small-$B_\perp$ region is very large and in the NLO case it causes a huge negative effect. It is clear that the fixed-order calculation is unable to describe the data. Resummation of the large logarithms is important [29].

As shown in Fig. 6 the large negative contributions come from the small-$B_\perp$ region ($B_\perp<0.02$). Resumming the leading and the next-to-leading logarithms the $B_\perp d\sigma/dB_\perp$ distribution is positive definite and we can expect that it is reasonably small in the small-$B_\perp$ region. On the other hand, Fig. 6 indicates that the NLO fixed-order calculation is a stable prediction in the large ($B_\perp>0.2$) region. Assuming that the all-order contribution of the $B_\perp<0.02$ region to the average value is small and changing the δ parameter we can make a better comparison of the data and NLO prediction. In Fig. 8

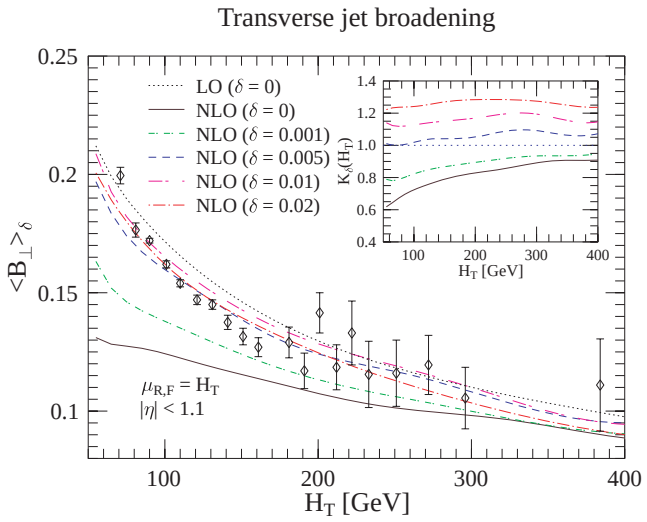

FIG. 8. (Color online) Average value of the $B_\perp$ event shape variable at $\delta=0$ at the LO and NLO levels for $\delta=0,0.001,0.005,0.01,0.02$. The scales were set to $\mu_{R,F}=H_T$. The markers (*diamonds*) and the error bars represent the CDF data [28] and their statistical error. The inset shows the *K* factors.

we can see that the $\langle B_\perp\rangle_{0.0}$ and the $\langle B_\perp\rangle_{0.001}$ NLO results suffer on the effect of the large logarithm but changing the δ parameter between 0.005 and 0.02 the NLO prediction is stable and hardly depends on the δ parameter and the agreement with the data is much better. The inset shows the $K_\delta=\langle B_\perp\rangle_\delta^{NLO}/\langle B_\perp\rangle_\delta^{LO}$ factor. For $0.005<\delta<0.02$ the NLO correction is positive, nearly constant, and is maximum 30%.

Of course this is not a precise analysis and without the resummation of the leading and next-to-leading logarithms the quantitative comparison of the current data and theory is impossible but it can help to understand the huge discrepancy between the data and NLO prediction. It also indicates that the NLO prediction can describe the data very well if $\delta>0.005$.

D. Subjet fractions

In this subsection we study the subjet multiplicities of the events. We use the exclusive $k_\perp$ algorithm [19]. The jets are defined in a two-step clustering procedure. The first step of the algorithm identifies the low-p_T scattering fragments and includes them in the beam jets, thus factorizing the hard scattering subprocess. The scale of the hard final state jets is E_{cut}, the stopping parameter of this clustering step. Defining the subjet resolution variable $y_{cut}=Q_0/E_{cut}$ the second step of the algorithm resolves the subjet structure of the hard final-state jets.

The *n*-subjet rate is defined by the ratio of the *n*-subjet cross section and the total cross section as

$$R_n(E_{cut},y_{cut})=\frac{\sigma_n(E_{cut},y_{cut})}{\sigma_{tot}(E_{cut})}, \tag{28}$$

where the σ is the total cross section defined by the sum of the *n*-jet cross section at the E_{cut} scale

$$\sigma_{tot}(E_{cut})=\sum_{n=2}^{\infty}\sigma_n(E_{cut})=\int_{E_{cut}}^{\infty}dE_{t2}\frac{d\sigma}{dE_{t2}}. \tag{29}$$

The E_{t2} variable is the smallest value of the E_{cut} resolution variable where the event has two jets. Using the similar event shape variables y_n and y_{n+1} of the second step we can define the exclusive subjet cross section at a given E_{cut} scale by

$$\sigma_n(E_{cut},y_{cut})=\int_{E_{cut}}^{\infty}dE_{t2}\left[\int_{y_{cut}}^{\infty}dy_n\frac{d\sigma}{dE_{t2}dy_n}-\int_{y_{cut}}^{\infty}dy_{n+1}\frac{d\sigma}{dE_{t2}dy_{n+1}}\right]. \tag{30}$$

In the fixed-order perturbation calculation we can calculate the three-subjet ratio at the NLO level $[R_3^{NLO}(E_{cut},y_{cut})]$ and the four-subjet ratio at the LO level $[R_4^{LO}(E_{cut},y_{cut})]$. From the definition of the *n*-subjet ratios we have the normalization condition

$$1=\sum_{i=2}^{\infty}R_n(E_{cut},y_{cut}). \tag{31}$$

Using this relation the two-subjet relation can be obtained at the next-to-next-to-leading order level (NNLO):

$$R_2^{NNLO}(E_{cut},y_{cut})=1-R_3^{NLO}(E_{cut},y_{cut})-R_4^{LO}(E_{cut},y_{cut})+\mathcal{O}(\alpha_s^3). \tag{32}$$

Analogously to the e^+e^- annihilation we can define the subjet multiplicity

$$N(E_{cut},y_{cut})=\sum_{n=2}^{\infty}nR_n(E_{cut},y_{cut}) \tag{33}$$

and at up to second order

$$N(E_{cut},y_{cut})=2+R_3^{NLO}(E_{cut},y_{cut})+2R_4^{LO}(E_{cut},y_{cut})+\mathcal{O}(\alpha_s^3). \tag{34}$$

The fixed-order perturbative predictions depend on the unphysical renormalization and factorization scales. In these calculations the scales are given on an event-by-event basis. We use the invariant mass of the two hard final-state jets found at the E_{t2} scale as the renormalization and factorization scales:

$$\mu_{R,F}^2=(p_1+p_2)^2. \tag{35}$$

Figure 9 shows the subjet ratios and subjet multiplicity. The result is given as a function of E_{cut} parameter and the base-ten logarithm of the subjet resolution variable. The distributions are plotted on the $10<E_{cut}<110$ GeV and $-3.9<\log_{10}(y_{cut})<0$ region. We can see that the subjet ratios are strongly dominated by the large logarithms in the low-E_{cut} and -y_{cut} regions. To be able to do any quantitative comparison to the experimental data in this region it is necessary to

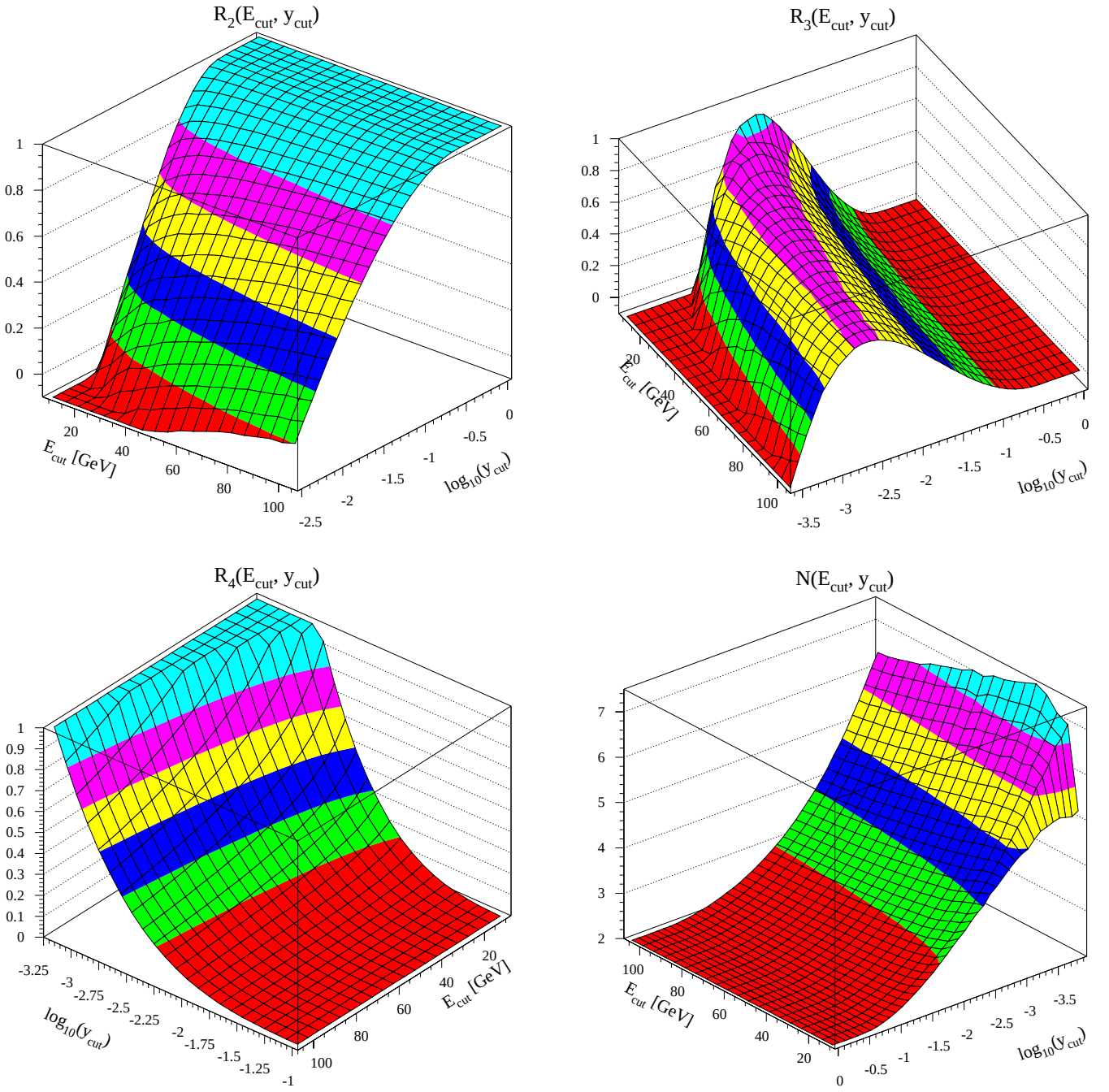

FIG. 9. (Color online) The fixed-order QCD prediction for the two-, three-, and four-jet subjet rates and for the subjet multiplicity. The two-jet rate is calculated at the NNLO, the three-jet rate is calculated at the NLO, and the four-jet at the LO levels.

sum at least the leading and next-to-leading logarithms at all order and match them to the fixed-order calculation.

IV. CONCLUSION

This paper dealt with the next-to-leading order calculation of three-jet observables in hadron-hadron collisions. We gave a modification of the original dipole method that it made possible to construct a Monte Carlo program for this process. We find that this modified dipole subtraction method was very useful from the point of the numerical calculation. The introduced phase space cut in the dipole term could reduce the evaluation time of subtraction terms and increase the numerical stability of the Monte Carlo integral by reducing the probability of the missed binning.

We calculated the transverse momentum distribution of the leading jet of the three-jet inclusive cross section using the inclusive $k_\perp$ an midcone algorithms. We found that the NLO correction can stabilize the theoretical prediction by reducing the renormalization and factorization scale dependences significantly. We also calculated the energy fraction distribution of the three-jet inclusive cross section. Compar-

ing the leading order result to the next-to-leading order result we found that the NLO corrections are negligible in these analyses.

We defined event shape variables in the transverse plane. We calculated the differential distribution of the transverse thrust and transverse jet broadening and the transverse energy dependence of the average values. We found that the size of the NLO correction is not too large and acceptable but at the edge of the available phase space the result suffers in the contribution of large logarithm. In this region a next-to-leading logarithmic approximation (NLL) matched with the fixed-order prediction can give a reasonable result. The average value of the transverse jet broadening was compared to the CDF data and we found that a comparison of the current data and theory without NLL resummation is impossible. Using a rough approximation in the small-$B_\perp$ region we were able to do some qualitative comparison between the data and NLO QCD prediction and we found reasonable good agreement.

We also calculated the subjet rates and subjet multiplicity using the exclusive $k_\perp$ algorithm. These quantities were defined in a way that mimicked an e^+e^- annihilationlike situation at hadron colliders. The result is very similar to what we have in e^+e^- annihilation. The subjet ratios are strongly dominated by the final-state large logarithm. Upgrading the fixed-order calculation with the next-to-leading logarithmic approximation this quantity may provide a sensitive measurement of the strong coupling at hadron colliders.

Recently two general methods have been developed by Banfi, Salam, and Zanderighi [29] and by Bonciani *et al.* [30] to carry out the next-to-leading logarithmic resummation for any observable. These methods can help us to improve our fixed-order calculation and to be able to make a more precise comparison between the data and theory.

ACKNOWLEDGMENTS

I wish to thank Zoltán Trócsányi for useful discussions and suggestions, as well as for collaboration on various elements of this project. This work was supported in part by the U.S. Department of Energy, contract DE-FG0396ER40969, by Research Training Network ''Particle Physics Phenomenology at High Energy Colliders,'' contract HPRN-CT-2000-00149, as well as by Hungarian Scientific Research Fund grant OTKA T-038240. I also thank the Institute Particle Physics Phenomenology (IPPP) at the University of Durham and the Fermi National Laboratory for making it possible for me to use their computer facilities.

[1] W.T. Giele, E.W.N. Glover, and D.A. Kosower, Nucl. Phys. **B403**, 633 (1993).
[2] Z. Kunszt and D.E. Soper, Phys. Rev. D **46**, 192 (1992).
[3] W.B. Kilgore and W.T. Giele, hep-ph/9903361; hep-ph/0009176; hep-ph/0009193.
[4] W.B. Kilgore and W.T. Giele, Phys. Rev. D **55**, 7183 (1997).
[5] Z. Nagy, Phys. Rev. Lett. **88**, 122003 (2002).
[6] Z. Trócsányi, Phys. Rev. Lett. **77**, 2182 (1996).
[7] Z. Nagy and Z. Trócsányi, Nucl. Phys. **B486**, 189 (1997).
[8] S. Frixione, Z. Kunszt, and A. Signer, Nucl. Phys. **B467**, 399 (1996).
[9] S. Catani and M.H. Seymour, Nucl. Phys. **B485**, 291 (1997).
[10] Z. Bern, L.J. Dixon, and D.A. Kosower, Phys. Rev. Lett. **70**, 2677 (1993).
[11] Z. Bern, L.J. Dixon, and D.A. Kosower, Nucl. Phys. **B437**, 259 (1995).
[12] Z. Kunszt, A. Signer, and Z. Trócsányi, Phys. Lett. B **336**, 529 (1994).
[13] J.F. Gunion and Z. Kunszt, Phys. Lett. **159B**, 167 (1985).
[14] J.F. Gunion and Z. Kunszt, Phys. Lett. B **176**, 163 (1986).
[15] J.F. Gunion and Z. Kunszt, Phys. Lett. B **176**, 477 (1986).
[16] J.G.M. Kuijf, Report No. rX-1335, Leiden, 1991.
[17] S.D. Ellis and D.E. Soper, Phys. Rev. D **48**, 3160 (1993).
[18] G.C. Blazey *et al.*, hep-ex/0005012.
[19] S. Catani, Y.L. Dokshitzer, M.H. Seymour, and B.R. Webber, Nucl. Phys. **B406**, 187 (1993).
[20] Z. Nagy and Z. Trocsanyi, Phys. Rev. D **59**, 014020 (1999).
[21] URL: http://www.cpt.dur.ac.uk/~nagyz/nlo++
[22] W.T. Giele, S.A. Keller, and D.A. Kosower, hep-ph/0104052.
[23] J. Pumplin *et al.*, J. High Energy Phys. **07**, 012 (2002).
[24] R. Kleiss and R. Pittau, Comput. Phys. Commun. **83**, 141 (1994).
[25] M.H. Seymour, Nucl. Phys. **B513**, 269 (1998).
[26] CDF Collaboration, F. Abe *et al.*, Phys. Rev. D **45**, 1448 (1992).
[27] CDF Collaboration, A. Brandl and S. Seidel, in the proceedings of 35th Rencontres de Moriond: QCD and High Energy Hadronic Interactions, Les Arcs, Savoie, France, 2000.
[28] CDF Collaboration, F. Abe *et al.*, Phys. Rev. D **44**, 601 (1991).
[29] A. Banfi, G.P. Salam, and G. Zanderighi, hep-ph/0304148.
[30] R. Bonciani, S. Catani, M.L. Mangano, and P. Nason, hep-ph/0307035.